

# Automated Distribution of Polarization-Entangled Photons Using Deployed New York City Fibers

Alexander N. Craddock<sup>✉,†</sup>, Anne Lazenby<sup>✉,†</sup>, Gabriel Bello Portmann, Rourke Sekelsky<sup>✉</sup>, Mael Flament<sup>✉</sup>, and Mehdi Namazi<sup>✉,\*</sup>

*Qunnect Inc., 141 Flushing Ave, Ste 1110, Brooklyn, New York 11205-1005, USA*



(Received 15 April 2024; revised 3 June 2024; accepted 14 June 2024; published 9 August 2024)

The distribution of high-fidelity high-rate entanglement over telecommunication infrastructure is one of the main paths toward large-scale quantum networks, enabling applications such as quantum encryption and network protection, blind quantum computing, distributed quantum computing, and distributed quantum sensing. However, the fragile nature of entangled photons operating in real-world fiber infrastructure has historically limited continuous operation of such networks. Here, we present a fully automated system capable of distributing polarization-entangled photons over a 34-km deployed fiber in New York City, achieving high rates of nearly  $5 \times 10^5$  pairs/s. Separately, we demonstrate a high fidelity of approximately 99% for rates up to  $2 \times 10^4$  pairs/s. Lastly, we achieve 15 days of continuous distribution, with a network up-time of 99.84%. Our work paves the way for practical deployment of always-on entanglement-based networks with rates and fidelity adequate for many current and future use cases.

DOI: [10.1103/PRXQuantum.5.030330](https://doi.org/10.1103/PRXQuantum.5.030330)

## I. INTRODUCTION

Entangled photons not only enhance the current capabilities of quantum links for applications in secure communication [1,2] but they are also fundamental for building large-scale quantum repeaters [3], distributed quantum computing [4–7], and distributed quantum sensing networks [8–10]. All such use cases rely on access to high-rate high-fidelity entanglement across the network. Therefore, the high-performance distribution of entanglement over quantum channels is essential for any future quantum network.

Given their weak environmental interactions and speed of propagation, photons are a natural choice as communication qubits. Among different types of photonic qubits, polarization states provide many advantages, such as ease of creation, manipulation, and measurement. Such states are also prime candidates for interfacing with atomic and ionic systems [11–13], paving the way toward larger scale distributed quantum networks.

Owing to the large amount of unused fiber available and the manageable optical losses over short ranges, telecom

fibers are a good choice for photonic quantum channels in metropolitan areas. However, environmental factors can affect fibers and cause changes to the polarization, typically represented as rotations in the Poincaré sphere [14]. These can be both wavelength and time dependent, and can in turn degrade fiber performance as a quantum channel for entanglement distribution. As a result, compared to other type of entanglement networks [15,16], the demonstrations of high-fidelity polarization-qubit distribution over extended periods of time are difficult [17]. However, due to the advantageous properties of these qubits, much research has been performed on their distribution. In the past two decades, the field has improved from the early-stage experiments over approximately 1-km fibers [18] to intercountry [17,19] and high-rate [20] links.

Up to now, much of the literature has focused on proof-of-principle experiments. However, practical entanglement networks will require stable long-term usable polarization-entanglement distribution with a high rate, high fidelity, and a high network up-time. Here, we report a series of measurements performed through buried fiber optics in New York City, using Qunnect's GothamQ test bed, shown in Fig. 1. We characterize the polarization-dispersion properties of the fibers in the GothamQ test bed. Then, using a narrow-band bichromatic polarization-entanglement source and an active polarization-compensating device, we demonstrate entanglement distribution with throughputs of nearly  $5 \times 10^5$  pairs/s over a 34-km-long fiber with a total loss of 17.4 dB, while at lower distribution rates, near  $2 \times 10^4$  pairs/s,

\*Contact author: mehdi@quconn.com

†These two authors contributed equally to this work.

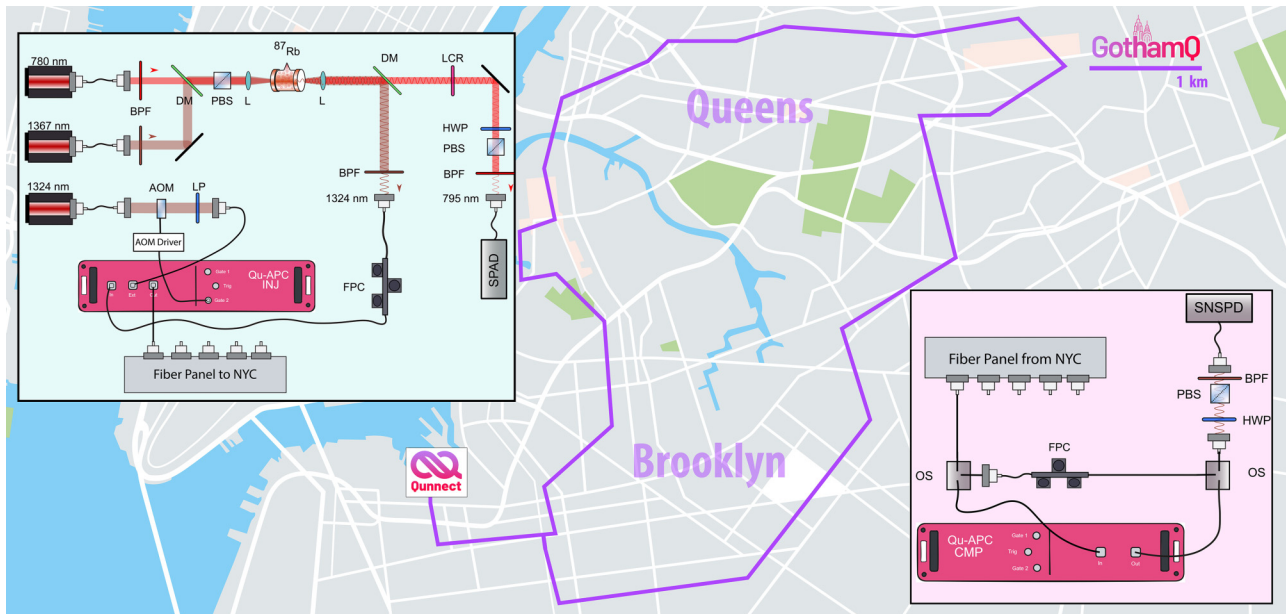


FIG. 1. The experimental setup for entanglement-distribution experiments. The background shows the path of the GothamQ fibers. The upper left (lower right) diagram shows the experimental apparatus prior to photons entering (exiting) the GothamQ fiber. PBS, polarizing beam splitter; DM, dichroic mirror; BPF, band-pass filter; LCR, liquid-crystal retarder; HWP, half-wave plate; L, lens; LP, linear polarizer; AOM, acousto-optic modulator; AOM Driver, AOM driver; Qu-APC INJ, Qu-APC injector; FPC, fiber polarization compensator; OS, optical switch; SPAD, single-photon avalanche detector; SNSPD, superconducting-nanowire single-photon detector.

we attain a fidelity of approximately 99%. We show that the entanglement-distribution system is capable of operating with high performance for over 15 days without any user input, maintaining a network up-time of 99.84%. In our scheme, the distributed 1324-nm telecom photon is entangled with a 795-nm near-infrared photon, which is detected locally. The 795-nm photon is natively bandwidth and wavelength compatible with rubidium atomic systems, such as quantum memories, quantum processors, and quantum sensors. Therefore, these experiments showcase practical and fully automated distribution of entangled photons at high rates and fidelity that is a step toward quantum repeating, distributed quantum computing, and distributed quantum sensing.

## II. FIBER POLARIZATION DISPERSION

First, we characterize the polarization dispersion of the fibers in the GothamQ network. For this work, we use a narrow-line-width laser (Thorlabs TLX3) with a tunable range, which covers nearly the entire telecom O band. For a given wavelength, we generate three polarization states,  $\{|H\rangle, |D\rangle, |R\rangle\}$ . We pass these through some fiber configuration and measure the resulting polarization states using a polarimeter (Thorlabs PAX1000IR2).

First, we assess the “instantaneous” polarization-dispersion behavior. For each of the three input polarizations, we sweep the wavelength of the tunable laser

from 1260 nm to 1350 nm with a 1-nm step, recording the polarization state at each wavelength. We perform this measurement for zero [21], one, two, and three fibers within GothamQ in series (or distances of approximately 0, 34, 68, and 102 km, respectively). We note that although the measurement is not truly instantaneous, we have verified that in each case the fiber was stable enough that this approximates an instantaneous measurement. Knowing the output and input states, we calculate the Poincaré-sphere rotation that the fiber configuration performs (see the Supplemental Material [22]). As seen in Figs. 2(a) and 2(b), in all cases we observe some level of dispersive polarization behavior. To better quantify the dispersion, we calculate the Poincaré-sphere rotation per unit nanometer, shown in Fig. 2(c). From this, we can see clearly that all the configurations that pass through GothamQ fibers exhibit a much higher level of polarization dispersion than the configuration that does not.

Given the above fiber behavior, we are able to make some inferences about the suitability of the fibers as quantum channels for distributing quantum entanglement. In Fig. 2(d), we calculate the fidelity for retaining a Bell state when one qubit is transmitted across a given fiber configuration, assuming that we have performed the appropriate correction on the receiving end to account for the Poincaré-sphere rotation at 1300 nm. By weighting curves such as those in Fig. 2(d) by a Gaussian with a given full width at half maximum (FWHM), we are able to make inferences about the fidelity of photon pairs where one

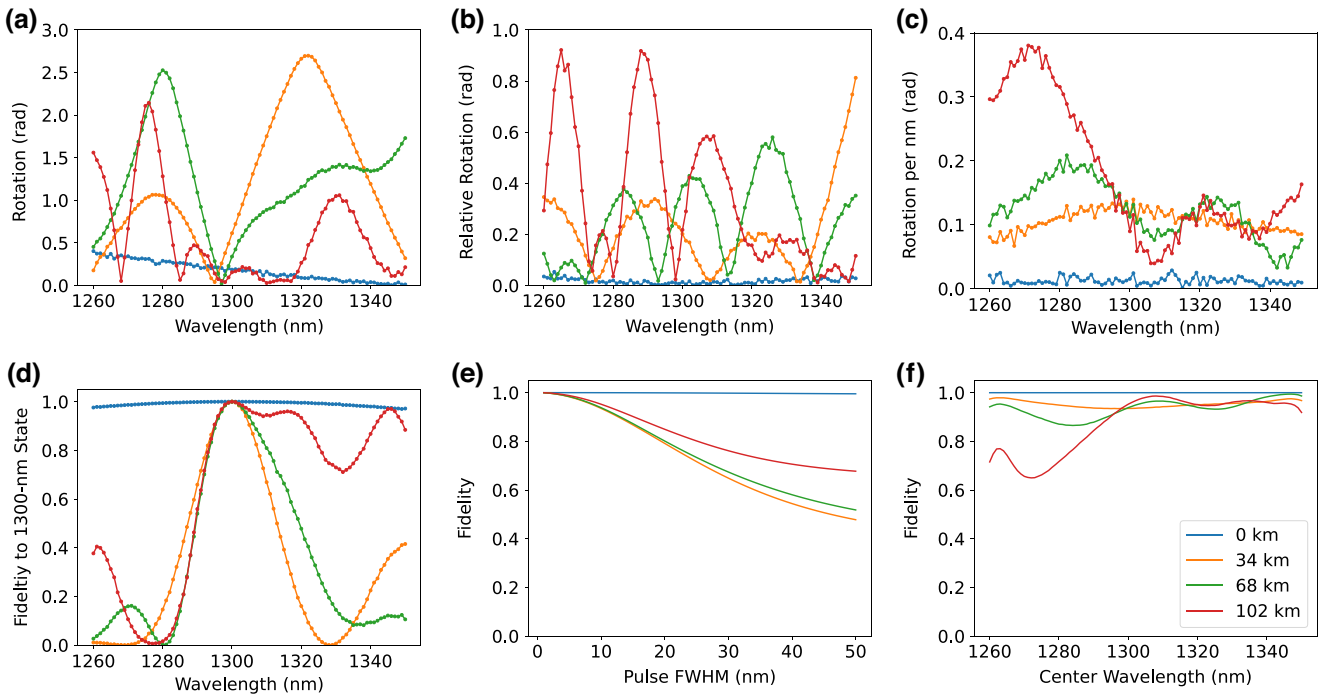


FIG. 2. “Instantaneous” fiber polarization-dispersion measurements. For each plot, the legend indicates the number of GothamQ fibers used for the measurement. (a) The Poincaré-sphere rotation as a function of the wavelength relative to the input. (b) The Poincaré-sphere rotation relative to the average rotation value as a function of the wavelength. (c) The Poincaré-sphere rotation between two wavelengths a nanometer apart. (d) The expected fidelity for a narrow-band Bell state where one qubit is passed through the fiber, assuming that at the exit of the fiber configuration, we have performed an operation to undo the Poincaré-sphere rotation for photons at 1300 nm. (e) The expected fidelity for a Bell state where one photon, with a center wavelength of 1300 nm, is passed through the fiber configuration as a function of the spectral width of the biphoton pair. (f) The expected fidelity for a Bell state for a biphoton pair with a spectral FWHM of 10 nm, as a function of the center wavelength of the photon that has passed through the fiber. In (a)–(d), the line is provided to guide the eye. The legend shown in (f) is shared by all plots.

photon is propagated along the GothamQ fibers. In Fig. 2(e), we show the expected fidelity as a function of the spectral FWHM of the biphoton pair, where the propagating photon has a center wavelength of 1300 nm, and in Fig. 2(f), we display the expected fidelity as a function of the central wavelength of the propagated photon for a biphoton pair with a 10-nm FWHM. We see that in all configurations, increasing the pulse bandwidth decreases the expected fidelity of the entangled state.

In addition to the “instantaneous” measurements, we measure the long-term fiber polarization-dispersion behavior, shown in Fig. 3. For the figure, we calculate the change in fidelity of a hypothetical narrow-band Bell state, where one photon is passed through the GothamQ fiber, as a function of the wavelength. As seen in the figure, polarization drift is experienced across the entire spectrum measured. Furthermore, the relative drift is wavelength dependent, implying that the behavior observed in Fig. 2 is time dependent. Such dependence on both wavelength and time demonstrates the need for active compensation at the same wavelength. Additionally, from the data it is clear that high-fidelity distribution of polarization qubits necessitates that the photons used be narrow band.

### III. ENTANGLEMENT DISTRIBUTION

#### A. Experimental setup

Next, we demonstrate entanglement distribution for pairs of photons where one is distributed in a buried fiber within New York City. The experimental setup for this is shown in Fig. 1.

We use a spontaneous four-wave mixing (SFWM) source based on warm atomic vapors to generate entangled bichromatic photon pairs. In the source, a 780-nm pump and 1367-nm coupling beam excite atoms within an enriched  $^{87}\text{Rb}$  vapor cell to the  $|6S_{1/2}\rangle$  state via the  $|5P_{3/2}\rangle$  intermediate state. From the doubly excited state, emission of a 1324-nm photon may occur, projecting a collective  $|5P_{1/2}\rangle$  excitation onto the vapor [23]. Subsequent decay of this collective excitation, which is highly directional, results in a photon at 795 nm. Due to the Zeeman structure of rubidium and the collinear pump and coupling polarization, the 1324 – 795 pairs are emitted in a polarization-entangled  $|\Phi_+\rangle = \frac{1}{\sqrt{2}}(|HH\rangle + |VV\rangle)$  Bell state [24]. For these experiments, we use a source setup similar to the one described in Ref. [25]. Additionally, we frequency lock the pump and coupling light to their optimal detunings,

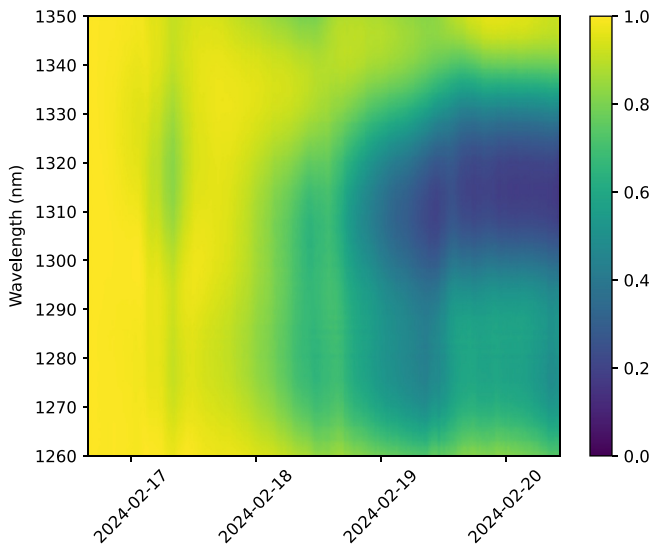


FIG. 3. The expected fidelity of a narrow-band Bell state over time as a function of the wavelength of the photon that has passed through one of the GothamQ fibers and time. In each case, the fidelity is calculated relative to the initial Poincaré state of the fiber for each wavelength.

as well as the vapor-cell temperature determined in Ref. [25]. Throughout the following, the pump and coupling powers are set to be equal and are adjusted to achieve the different pair rates shown. An advantage of this source is that it natively produces narrow-band (line width less than 1 GHz) polarization-entangled biphotons. From Fig. 2, this should mean that the fidelity of the entangled state after propagation should not be bounded by the photon line width.

To preserve the fidelity of the entangled state as photons are passed through the metropolitan fiber, we use our automated-polarization-compensation (APC) devices. This allows us to perform active polarization compensation, in contrast to previous work [17,19,20]. The APC operates as a pair, with an injector and a compensator at either end of the fiber. The APC injector produces a sequence of classical states with well-defined polarization, created using a polarizer followed by an electro-elasto-optic modulator (EEOM). We pass the classical pulses down the fiber to be stabilized to the APC compensator. The compensator contains an EEOM (with a modulation bandwidth of approximately 120 kHz) and a fast polarimeter ( $10^4$  measurements per second). The compensator EEOM contains four independently adjustable crystals with optical axes orientated at  $-45^\circ$ ,  $0^\circ$ ,  $90^\circ$ , and  $45^\circ$ , allowing the device to perform any possible Poincaré-sphere rotation. We initialize the pair by taking a reference measurement with the polarimeter, after which, the compensator adjusts its EEOM to ensure subsequent pulse sets from the injector match the reference. We use time-division multiplexing to mix the classical pulse sequence

with light passed to the input port of the injector, via a set of optical switches. For all the measurements shown, we trigger the APC compensation cycle approximately every 20 s. In each compensation cycle, the fidelity is first measured by comparing the current state of the fiber to the reference. If it is found to exceed a trigger threshold (set here to be 99%), then the compensation cycle finishes. If it is below the threshold, we utilize a gradient-descent algorithm to adjust the compensator EEOM until it exceeds an optimization threshold (also set here to be 99%). The compensation cycle takes between 30 and 1000 ms, depending on the polarization rotation that has occurred on the fiber. For the data shown, adjustment of the compensator EEOM has been required approximately every 45 min. Further details, and diagrams of the APC devices, can be found in the Supplemental Material [22].

As discussed earlier, close matching of the wavelength of the classical and quantum light is required to ensure good polarization compensation of the fiber for the quantum light. Therefore, we use a 1324-nm laser source as our classical light for the APC injector, verified with a wave meter to be within a nanometer of the signal photons produced by the source. The laser is left free running throughout the experiment. After coupling the classical light into fiber, we pass the light through a fiber-based acousto-optic modulator (AOM). The AOM is on-off controlled by the APC injector to shutter the classical light when active compensation is not occurring. Along with the built-in optical switches, this minimizes the noise present at the telecom measurement station due to the APC. After the AOM, we use an in-fiber polarizer to ensure a well-defined input polarization for the classical field passed to the APC injector.

For this experiment, we couple the 1324-nm telecom photons produced by the source into a fiber attached to the input port of the APC injector, which is in turn connected to the buried 34-km-long metropolitan fiber, shown in Fig. 1. After traveling through the metropolitan fiber, we pass the telecom photons to a fiber switch. From the switch, we either pass the photons to the APC compensator or to a fiber path that bypasses the compensator completely. A further switch recombines the paths and sends the photons for polarization analysis. With both switches, we are able to toggle between compensating and not compensating for drifts in the metropolitan fiber.

For analysis of the entangled state after fiber transit, we use a measurement station for each of the two source-photon wavelengths. In both cases, the measurement station consists of a half-wave plate and a polarizing beam splitter. We perform polarization measurements for the 795-nm photons prior to fiber coupling at the source setup. For the 1324-nm photons, we use an independent measurement-station setup that includes a band-pass filter (50-nm FWHM). This helps to minimize noise that may have accumulated in the metropolitan

fiber. While full two-photon tomography requires both a quarter- and half-wave plate for both photons for polarization analysis [26], we use a method (see the Supplemental Material [22]) that allows us to bound the entangled-state fidelity using only measurements of the coincidences in the  $\{|HH\rangle, |HV\rangle, |VH\rangle, |VV\rangle, |DD\rangle, |DA\rangle, |AD\rangle, |AA\rangle\}$  modes.

For the 1324-nm photons, we use a pair of polarization controllers: one prior to the APC injector input and one on the uncompensated path between the two fiber switches. The initial polarization rotation performed by the metropolitan fiber, as well as other shorter fibers within the setup, is unknown. We use the fiber polarization controllers, along with a liquid-crystal retarder (LCR) on the source setup to undo this initial rotation for the compensated and uncompensated paths. For the two experiments presented later, the LCR and controllers have been calibrated prior to any data being taken and then the values fixed for the duration of the experiment.

We detect the 795-nm photons using a set of single-photon avalanche photodiodes and the 1324-nm photons using a superconducting-nanowire single-photon detector (SNSPD) (approximately 350-ps and approximately 90-ps timing jitters, and 68% and 90% detection efficiencies, respectively). We find that the metropolitan fiber has a loss of 14.45 dB. Along with the other losses due to other elements (see the Supplemental Material [22]), the total loss from the source to the input of the telecom measurement station is 17.46 dB.

### B. Rate versus fidelity

Here, we explore the dependence of the entanglement fidelity on the fiber pair throughput. For this experiment, we adjust the pump and coupling powers to change the source entangled-pair-generation rate. Given the probabilistic nature of the entangled-pair source used, we expect the pair cross-correlation, and therefore the entangled-state fidelity, to decrease as the pair generation rate is increased (see the Supplemental Material [22]). At each generation rate, we take the fidelity-bounding measurements (described above) approximately every 4 min for a total of 4 h. For each fidelity-bounding measurement, we calculate the highest lower bound and the lowest upper bound (see the Supplemental Material [22]) on the fidelity to the  $|\phi_+\rangle = |HH\rangle + |VV\rangle/\sqrt{2}$  Bell state.

The average and standard deviation on the lower bounds over the 4-h measurement duration are shown in Fig. 4 for various entangled-pair rates. We note that we can only bound the fidelity due to the measurement method chosen and that the bounds do not arise purely from experimental uncertainties (see the Supplemental Material [22]). At the maximum pump and control power available for this experiment, we can achieve an end-to-end pair distribution rate of approximately  $5 \times 10^5$ . At this throughput, we

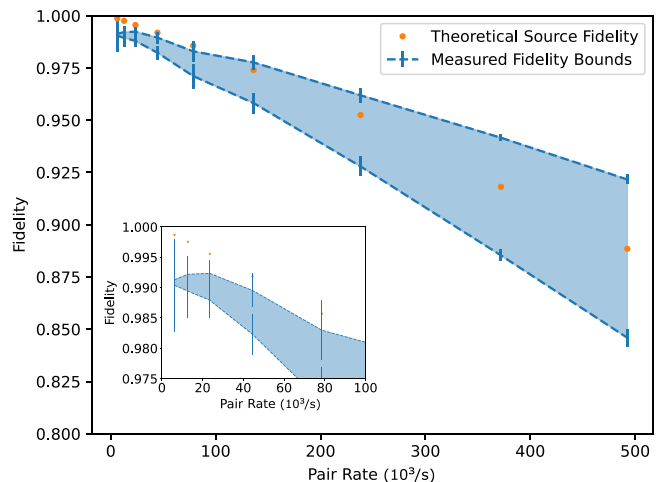


FIG. 4. The fidelity to the  $|\phi_+\rangle = |HH\rangle + |VV\rangle/\sqrt{2}$  Bell state as a function of the throughput pair rate (after 1324-nm photons are passed through a single GothamQ fiber). For each pair rate, an hour-long data set has been taken. The inset shows an enlargement of the low-rate behavior. The fidelity bounds (see the Supplemental Material [22]) are the mean over the data set and the error bars are from statistical uncertainties. The theoretical fidelity is calculated as  $1 - 3/2(1 + g_{SI})$  (for derivation, see the Supplemental Material [22]).

have experimentally bounded the entangled-state fidelity to be  $>0.84$ . However, we believe that the state fidelity should be source limited to approximately 0.88. For Fig. 4, the pair rate has been calculated by summing the number of coincidences observed in the  $\{|HH\rangle, |VV\rangle, |HV\rangle, |VH\rangle\}$  modes and dividing out peak detection efficiencies.

The ability to reach such high rates at a high fidelity over real-life metropolitan networks opens up the path for practical deployment of entanglement-based quantum-secured communication links. The high-fidelity distribution of entangled photons is a key step toward networked quantum computing and distributed quantum sensing over deployed fibers. While for high pair generation rates the limit on the fidelity is from the source itself, at lower throughput rates, around  $2 \times 10^4$  pairs/s, we can reach a fidelity of approximately 0.99, which is consistent with the thresholds set for the APC process. The achievement of such high fidelity for polarization-entanglement distribution not only surpasses all previous polarization-based deployments but, to the best of our knowledge, it is on par with the state-of-the-art for time-bin- and time-energy-based entanglement networks [15,16].

### C. Long-term usability measurement

Another important aspect of a practical quantum network is the long-term uninterrupted distribution of photon pairs without the need for manual intervention. Previous works [17] have shown great progress toward this goal but have still required relatively time-consuming manual

or automatic optimizations, which in turn have affected the overall network up-time. Here, we demonstrate the long term usability of the entangled pairs when the 1324-nm photons from the source are transmitted over the 34-km metropolitan fiber. For this experiment, the pump and coupling powers are fixed to produce approximately  $2 \times 10^5$  pairs/s after passing through fiber. Our experimental loop consists of taking fidelity-bounding measurements both for a path compensated by the APC and for an uncompensated path for comparison. The experimental cycle is repeated approximately every 4 min for over 15 days. Similar to the previous experiment, we calculate the highest lower and lowest upper bound on the fidelity of the state, in both the compensated and uncompensated case, to the  $|\phi_+\rangle = |HH\rangle + |VV\rangle/\sqrt{2}$  Bell state.

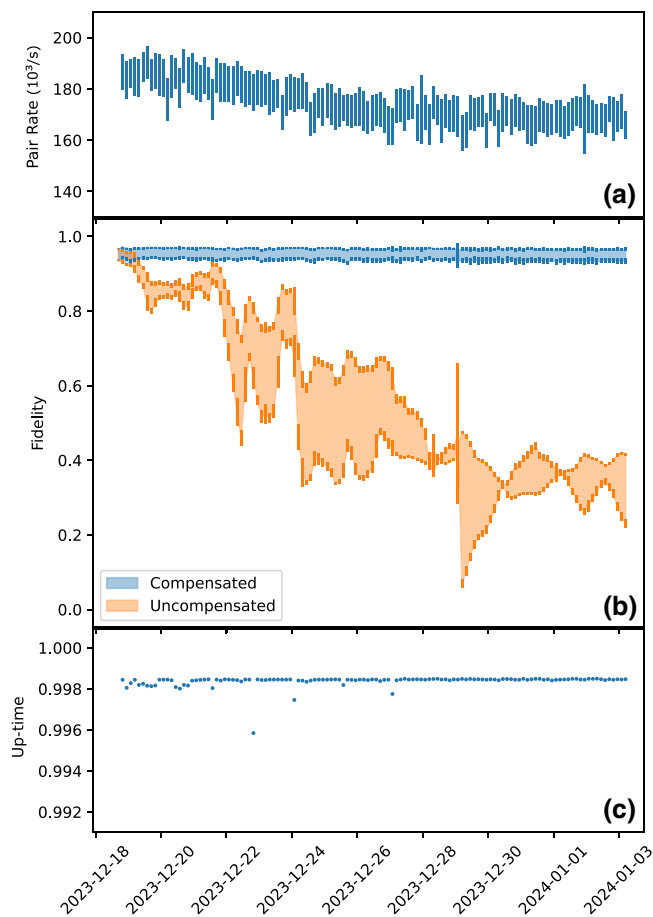


FIG. 5. The results of long-term usability measurement. (a) The pair rate observed through the compensated path. (b) The fidelity bounds (see the Supplemental Material [22]) for the compensated and uncompensated paths. (c) The up-time (the time for which entangled pairs are being actively distributed). In all plots, we have performed a 3-h trailing average for ease of viewing. The uncertainties quoted come from the statistical deviation within the 3-h averaging windows.

In Fig. 5(a), we show the entangled-pair rate (calculated similarly to Fig. 4) that has passed through the metropolitan fiber. The observed downward trend in the pair rate over the measurement period has been recovered upon completion by adjusting the polarization being sent to the SNSPD. Therefore, we believe that the actual pair rate was stable over the course of the measurement.

As seen in Fig. 5(b), the state fidelity for the path compensated by the APC is approximately constant over the 15-day measurement, with average lower and upper bounds of 0.937(7) and 0.967(4), respectively. Similar to before, we believe at these rates the fidelity should be limited by the source to approximately 95%. In contrast, the path that is uncompensated experiences significant fluctuations over the course of the measurement, with slow drifts observed in addition to discrete jumps.

In Fig. 5(c), we show the up-time for the data run. We see that the above results are achieved with a network up-time consistently above 99%, with a total up-time of 99.84% over the 15-day run. These results demonstrate highly stable distribution of high-rate high-fidelity polarization-entangled photons under real-world conditions, opening up the path for round-the-clock use of quantum entanglement within telecommunication infrastructure.

#### IV. CONCLUSIONS

The robust distribution of entanglement with high-rate and fidelity across deployed fibers will be critical for the development of the quantum Internet. Here, we have presented data from a quantum test bed in New York City, GothamQ, demonstrating progress toward a fully automated practical entanglement network. Using 34 km of deployed fiber in the city, we have showcased the possibility of distributing polarization-entangled photons with a fidelity up to 99% and rates as high as  $5 \times 10^5$  pairs/s. Additionally, we have presented the long-term usability of the network, achieving high network up-time (>99.5%) for an extended period of operation (15 days). This demonstration shows that robust, high-up-time, round-the-clock operation of entanglement-distribution networks is attainable for practical use cases. Furthermore, the native compatibility of the 795-nm photons used with atomic systems [25] opens the door to practically all warm-atom-based quantum repeating, sensing, and distributed computing over telecom fibers.

#### ACKNOWLEDGMENTS

We thank Thorlabs for generously lending us a TLX3 to perform the fiber polarization-dispersion measurements. We thank the Qunnect Inc. team, especially Noel Goddard, Yang Wang, and Felipe Giraldo, for their insights and help with manuscript preparation.

- [1] A. K. Ekert, Quantum cryptography based on Bell's theorem, *Phys. Rev. Lett.* **67**, 661 (1991).
- [2] C. H. Bennett, G. Brassard, and N. D. Mermin, Quantum cryptography without Bell's theorem, *Phys. Rev. Lett.* **68**, 557 (1992).
- [3] K. Azuma, S. E. Economou, D. Elkouss, P. Hilaire, L. Jiang, H.-K. Lo, and I. Tzitrin, Quantum repeaters: From quantum networks to the quantum Internet, *Rev. Mod. Phys.* **95**, 045006 (2023).
- [4] C. Monroe, R. Raussendorf, A. Ruthven, K. R. Brown, P. Maunz, L.-M. Duan, and J. Kim, Large-scale modular quantum-computer architecture with atomic memory and photonic interconnects, *Phys. Rev. A* **89**, 022317 (2014).
- [5] S. Pirandola and S. L. Braunstein, Physics: Unite to build a quantum Internet, *Nature* **532**, 169 (2016).
- [6] S. Wehner, D. Elkouss, and R. Hanson, Quantum Internet: A vision for the road ahead, *Science* **362**, eaam9288 (2018).
- [7] H. J. Kimble, The quantum Internet, *Nature* **453**, 1023 (2008).
- [8] Z. Eldredge, M. Foss-Feig, J. A. Gross, S. L. Rolston, and A. V. Gorshkov, Optimal and secure measurement protocols for quantum sensor networks, *Phys. Rev. A* **97**, 042337 (2018).
- [9] E. T. Khabiboulline, J. Borregaard, K. De Greve, and M. D. Lukin, Optical interferometry with quantum networks, *Phys. Rev. Lett.* **123**, 070504 (2019).
- [10] T. J. Proctor, P. A. Knott, and J. A. Dunningham, Multi-parameter estimation in networked quantum sensors, *Phys. Rev. Lett.* **120**, 080501 (2018).
- [11] T. Wilk, S. C. Webster, A. Kuhn, and G. Rempe, Single-atom single-photon quantum interface, *Science* **317**, 488 (2007).
- [12] A. Stute, B. Casabone, P. Schindler, T. Monz, P. O. Schmidt, B. Brandstätter, T. E. Northup, and R. Blatt, Tunable ion-photon entanglement in an optical cavity, *Nature* **485**, 482 (2012).
- [13] A. Craddock, J. Hannegan, D. Ornelas-Huerta, J. Siverns, A. Hachtel, E. Goldschmidt, J. Porto, Q. Quraishi, and S. Rolston, Quantum interference between photons from an atomic ensemble and a remote atomic ion, *Phys. Rev. Lett.* **123**, 213601 (2019).
- [14] E. Bersin, *et al.*, Development of a Boston-area 50-km fiber quantum network testbed, *Phys. Rev. Appl.* **21**, 014024 (2024).
- [15] Y. Pelet, G. Sauder, M. Cohen, L. Labonté, O. Alibart, A. Martin, and S. Tanzilli, Operational entanglement-based quantum key distribution over 50 km of field-deployed optical fibers, *Phys. Rev. Appl.* **20**, 044006 (2023).
- [16] E. Fitzke, L. Bialowons, T. Dolejsky, M. Tippmann, O. Nikiforov, T. Walther, F. Wissel, and M. Gunkel, Scalable network for simultaneous pairwise quantum key distribution via entanglement-based time-bin coding, *PRX Quantum* **3**, 020341 (2022).
- [17] S. P. Neumann, A. Buchner, L. Bulla, M. Bohmann, and R. Ursin, Continuous entanglement distribution over a transnational 248 km fiber link, *Nat. Commun.* **13**, 6134 (2022).
- [18] A. Poppe, A. Fedrizzi, R. Ursin, H. R. Böhm, T. Lorünser, O. Maurhardt, M. Peev, M. Suda, C. Kurtsiefer, H. Weinfurter, T. Jennewein, and A. Zeilinger, Practical quantum key distribution with polarization entangled photons, *Opt. Express* **12**, 3865 (2004).
- [19] S. Wengerowsky, S. K. Joshi, F. Steinlechner, J. R. Zichi, S. M. Dobrovolskiy, R. van der Molen, J. W. N. Los, V. Zwiller, M. A. M. Versteegh, A. Mura, D. Calonico, M. Inguscio, H. Hübel, L. Bo, T. Scheidl, A. Zeilinger, A. Xuereb, and R. Ursin, Entanglement distribution over a 96-km-long submarine optical fiber, *Proc. Natl. Acad. Sci. USA* **116**, 6684 (2019).
- [20] L. Shen, C. H. Chow, J. Y. X. Peh, X. J. Yeo, P. K. Tan, and C. Kurtsiefer, Distributing polarization-entangled photon pairs with high rate over long distances through standard telecommunication fiber, *Phys. Rev. Appl.* **18**, 044075 (2022).
- [21] This configuration does not pass through GothamQ but the light traverses approximately 20 m of fiber common between all the other measurements.
- [22] See the Supplemental Material at <http://link.aps.org-supplemental/10.1103/PRXQuantum.5.030330> for further details on the APC, derivation of fidelity bounding equations, loss budget for telecom photon, and derivation of Poincaré sphere rotation calculations.
- [23] O. Davidson, R. Finkelstein, E. Poem, and O. Firstenberg, Bright multiplexed source of indistinguishable single photons with tunable GHz-bandwidth at room temperature, *New J. Phys.* **23**, 073050 (2021).
- [24] R. T. Willis, F. E. Becerra, L. A. Orozco, and S. L. Rolston, Photon statistics and polarization correlations at telecommunications wavelengths from a warm atomic ensemble, *Opt. Express* **19**, 14632 (2011).
- [25] A. N. Craddock, Y. Wang, F. Giraldo, R. Sekelsky, M. Flament, and M. Namazi, High-rate subgigahertz linewidth bichromatic entanglement source for quantum networking, *Phys. Rev. Appl.* **21**, 034012 (2024).
- [26] D. F. V. James, P. G. Kwiat, W. J. Munro, and A. G. White, Measurement of qubits, *Phys. Rev. A* **64**, 052312 (2001).